

Vertical polarization-induced doping InN/InGaN heterojunction tunnel FET with hetero T-shaped gate

Yuan-Hao He(何元浩), Wei Mao(毛维), Ming Du(杜鸣), Zi-Ling Peng(彭紫玲), Hai-Yong Wang(王海永), Xue-Feng Zheng(郑雪峰), Chong Wang(王冲), Jin-Cheng Zhang(张进成), Yue Hao(郝跃)
Citation: Chin. Phys. B, 2021, 30 (**5**): 058501. DOI: 10.1088/1674-1056/abd73f
Journal homepage: http://cpb.iphy.ac.cn; http://iopscience.iop.org/cpb

What follows is a list of articles you may be interested in

Improved 4H-SiC UMOSFET with super-junction shield region

Pei Shen(沈培), Ying Wang(王颖), Xing-Ji Li(李兴冀), Jian-Qun Yang(杨剑群), Cheng-Hao Yu(于成浩), Fei Cao(曹菲)
Chin. Phys. B, 2021, 30 (**5**): 058502. DOI: 10.1088/1674-1056/abd740

A new algorithm based on *C-V* characteristics to extract the epitaxy layer parameters for power devices with the consideration of termination

Jiupeng Wu(吴九鹏), Na Ren(任娜), and Kuang Sheng(盛况)
Chin. Phys. B, 2021, 30 (**4**): 048505. DOI: 10.1088/1674-1056/abcf9e

Novel Si/SiC heterojunction lateral double-diffused metal-oxide semiconductor field-effect transistor with p-type buried layer breaking silicon limit

Baoxing Duan(段宝兴), Xin Huang(黄鑫), Haitao Song (宋海涛), Yandong Wang(王彦东), and Yintang Yang(杨银堂)
Chin. Phys. B, 2021, 30 (**4**): 048503. DOI: 10.1088/1674-1056/abcf45

Influences of supply voltage on single event upsets and multiple-cell upsets in nanometer SRAM across a wide linear energy transfer range

Yin-Yong Luo(罗尹虹), Wei Chen(陈伟), Feng-Qi Zhang(张凤祁), and Tan Wang(王坦)
Chin. Phys. B, 2021, 30 (**4**): 048502. DOI: 10.1088/1674-1056/abcf38

New DDSCR structure with high holding voltage for robust ESD applications

Zi-Jie Zhou(周子杰), Xiang-Liang Jin(金湘亮), Yang Wang(汪洋), and Peng Dong(董鹏)
Chin. Phys. B, 2021, 30 (**3**): 038501. DOI: 10.1088/1674-1056/abd38f

---

Vertical polarization-induced doping InN/InGaN heterojunction tunnel FET with hetero T-shaped gate*

Yuan-Hao He(何元浩)†, Wei Mao(毛维)†,‡, Ming Du(杜鸣)†, Zi-Ling Peng(彭紫玲), Hai-Yong Wang(王海永), Xue-Feng Zheng(郑雪峰), Chong Wang(王冲), Jin-Cheng Zhang(张进成), and Yue Hao(郝跃)

Key Laboratory of Ministry of Education for Wide Band-Gap Semiconductor Materials and Devices, School of Microelectronics, Xidian University, Xi'an 710071, *China*

(Received 21 August 2020; revised manuscript received 18 November 2020; accepted manuscript online 30 December 2020)

A novel vertical InN/InGaN heterojunction tunnel FET with hetero T-shaped gate as well as polarization-doped source and drain region (InN-Hetero-TG-TFET) is proposed and investigated by Silvaco-Atlas simulations for the first time. Compared with the conventional physical doping TFET devices, the proposed device can realize the P-type source and N-type drain region by means of the polarization effect near the top InN/InGaN and bottom InGaN/InN heterojunctions respectively, which could provide an effective solution of random dopant fluctuation (RDF) and the related problems about the high thermal budget and expensive annealing techniques due to ion-implantation physical doping. Besides, due to the hetero T-shaped gate, the improvement of the on-state performance can be achieved in the proposed device. The simulations of the device proposed here in this work show I_{ON} of 4.45×10^{-5} A/μm, I_{ON}/I_{OFF} ratio of 10^{13}, and SS_{avg} of 7.5 mV/dec in InN-Hetero-TG-TFET, which are better than the counterparts of the device with a homo T-shaped gate (InN-Homo-TG-TFET) and our reported lateral polarization-induced InN-based TFET (PI-InN-TFET). These results can provide useful reference for further developing the TFETs without physical doping process in low power electronics applications.

Keywords: InGaN TFET, hetero T-shaped gate, polarization-doped source and drain

PACS: 85.30.De, 85.30.Tv, 85.30.Mn **DOI:** 10.1088/1674-1056/abd73f

1. Introduction

As the size of semiconductor devices continues to shrink into the nanoscale, the problems of short channel effects (SCEs) and off-state leakage in traditional MOSFETs are becoming more and more serious. Especially due to thermal emission mechanism, the subthreshold slope (*SS*) cannot break through the limit of 60 mV/decade, which is not suitable effectively for energy-efficient and low-voltage applications.[1–4] Tunneling field-effect transistors (TFETs) have been considered as a suitable alternative to nanoscale MOSFETs in future low power electronics applications.[1] Based on the quantum band-to-band tunneling (BTBT) mechanism, TFETs could realize steeper average subthreshold swing (SS_{avg} < 60 mV/decade), lower off-state leakage current (I_{OFF}), and great immune to short channel effects in comparison with conventional nanoscale MOSFETs.[5–7]

However, there still exist many problems needed to be solved during the application of TFETs with conventional physical doping, such as the high thermal budget and expensive annealing techniques due to ion-implantation physical doping, and the random dopant fluctuation (RDF), which can deteriorate the device performances.[8–12] Recently, various dopingless TFETs have been proposed based on the charge-plasma concept,[13–16] which demonstrates an effective way to realize TFETs without physical doping. And based on the polarization effect near III-nitride-based heterointerfaces,[17–21] the lateral polarization-induced InN-based TFETs (PI-InN-TFET) have been demonstrated by our group.[22] This also opens a new path to the further development of TFETs without physical doping processing. In addition, in order to improve the on-state current, some effective methods, such as gate engineering, energy band engineering, and source-pocket doping[23–30] have been proposed and investigated.

In this paper, a novel vertical polarization-induced doping InN/InGaN heterojunction tunnel FET with hetero T-shaped gate (InN-Hetero-TG-TFET) is proposed and investigated. This device features a polarization-doped drain and source combined with a hetero T-shaped gate, which is different from the conventional vertical tunnel FET with physical doping. Based on these features, the problems about the random dopant fluctuation and the high thermal annealing techniques could be avoided, and the on-state performance could be improved. Comparative analyses between the InN-Hetero-TG-TFET and the vertical polarization-induced doping InN/InGaN heterojunction tunnel FET with homo T-shaped gate (InN-Homo-TG-TFET) are conducted. And the systematical simulations of the influence of the work-function and position of hetero T-shaped gate on the performance of the InN-Hetero-TG-TFET are carried out by Silvaco-Atlas. These results demonstrate the excellent characteristics of the

*Project supported by the Key Research and Development Program of Shaanxi Province, China (Grant No. 2020ZDLGY03-05) and the National Natural Science Foundation of China (Grant No. 61574112).

†These authors contributed equally to this work.

‡Corresponding author. E-mail: mwxidian@126.com

© 2021 Chinese Physical Society and IOP Publishing Ltd

InN-Hetero-TG-TFET in comparison with the InN-Homo-TG-TFET and our reported lateral polarization-induced InN-based TFET (PI-InN-TFET), which indicates a great potential of the proposed InN-Hetero-TG-TFET in the low power applications.

2. Device structure and simulation parameters

Figure 1 shows the schematic cross-section of InN-Homo-TG-TFET (Fig. 1(a)) and InN-Hetero-TG-TFET (Fig. 1(b)). The T-shaped gate and dual channel are used in both devices, and both the devices have the same main dimensions. The main parameters of the InN-Homo-TG-TFET and proposed InN-Hetero-TG-TFET are shown in Table 1. Both devices use the vertical InN/$In_xGa_{1-x}N$/InN layer structure to form the drain and source region without physical doping. Furthermore, the source and drain are set to be at both sides of devices, which is compatible with the planar fabrication process of the GaN-based HEMTs. The InN-Hetero-TG-TFET features a hetero T-shaped gate consisting in two metals with different metal work-functions applied to modulate the $In_xGa_{1-x}N$ band between hetero gate at different gate bias voltages, which could be used to control the tunneling distance and thus improving the on-state current and reducing the ambipolar leakage current.

Devices are simulated with two-dimensional numerical software Silvaco-Atlas. A Poisson's equation is used to solve self-consistently the carrier current continuity equations. Device models in this paper are mainly based on our early research.[16,22,31] The nonlocal BTBT model is used for the consideration of the spatial variation of the energy band and the more accurate calculation of the tunneling process. The Shockley–Read–Hall and Auger recombination models are adopted to consider the effect of carrier recombination. Besides, band-gap narrowing model, concentration-dependent and field-dependent mobility models are also used. Main material parameters in simulations are given in Table 2.

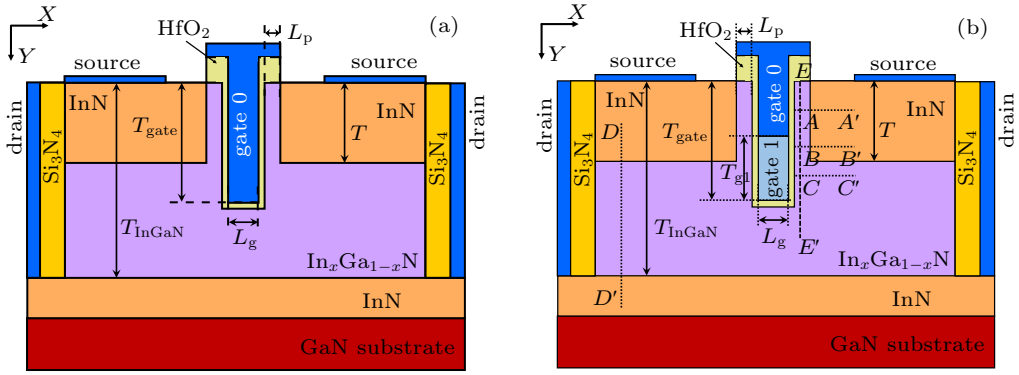


Fig. 1. Schematic cross-section of (a) InN-Homo-TG-TFET and (b) InN-Hetero-TG-TFET.

Table 1. Design parameters used in simulations.

Parameters	InN-Homo-TG-TFET	InN-Hetero-TG-TFET
Source InN thickness T (nm)	10	10
Channel InGaN thickness T_{InGaN} (nm)	67	67
Total gate trench thickness T_{gate} (nm)	30	30
$In_xGa_{1-x}N$ length between gate L_p (nm)	3	3
Gate HfO_2 thickness (nm)	2	2
In fraction x	0.8	0.8
Gate length L_g (nm)	10	10
Gate work-function (eV)	$\varphi = 4.8/5.65$	$\varphi_0 = 5.65$ $\varphi_1 = 4.80$
Gate1 thickness T_{g1} (nm)	0	23

Table 2. Material parameters in simulations.[17,32,33]

Parameters	InN	$In_xGa_{1-x}N$
Band gap E_g (eV)	0.7	$1.4x^2 - 4.12x + 3.42$
Band offset ΔE_c (eV)	0	$0.98x^2 - 2.884x + 1.904$
Electron effective mass m_e (m_0)	0.07	$0.2 - 0.13x$
Hole effective mass m_h (m_0)	0.27	$0.46 - 0.19x$
Permittivity (ε_r)	15.3	$8.9 + 6.4x$
Electron mobility μ_e ($cm^2/V{\cdot}s$)	1500	1500
Hole mobility μ_h ($cm^2/V{\cdot}s$)	20	20

The detailed distributions of the polarization-induced carrier concentration in the InN-Hetero-TG-TFET can be observed in Fig. 2. As shown in the figure, the source region exhibits the P-type doping with the peak hole concentration near the top InN/InGaN junction, while the drain region exhibits the N-type doping with the peak electron concentration near the bottom InGaN/InN junction. Figure 3 displays the vertical distribution diagram of carrier concentration and polarization charge concentration in the source region and drain region corresponding to Fig. 2 along the line D–D' in Fig. 1(b).

As shown in Fig. 3, there is a great negative polarization charge density peak σ_{top} near the top InN/InGaN junction because of the spontaneous and piezoelectric polarization effect, which indicates a large number of net negative bound polarization charges are located near the junction. Based on the local neutralization principle, holes are consequently induced to neutralize these negative bound sheet charges, which thus forms the P-type doping of source region. A positive polarization charge density peak σ_{bottom} appears near the bottom InGaN/InN junction, and thus the electrons can be induced near the bottom InGaN/InN junction in the same way, which forms N-type doping of drain region. The results are consistent with experimental results reported previously.[34]

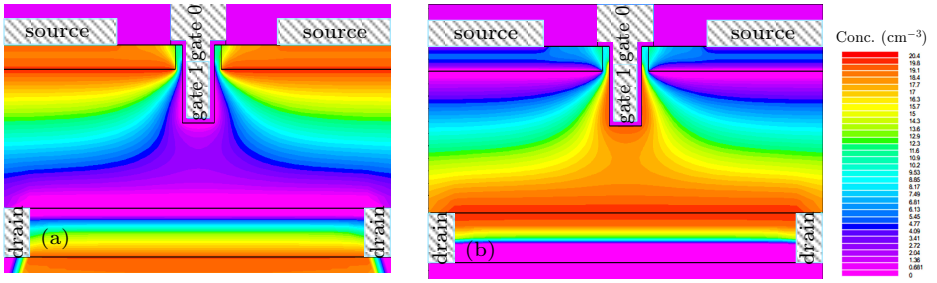


Fig. 2. Distribution of polarization-induced (a) hole concentration (Conc.) and (b) electron concentration in InN-Hetero-TG-TFET.

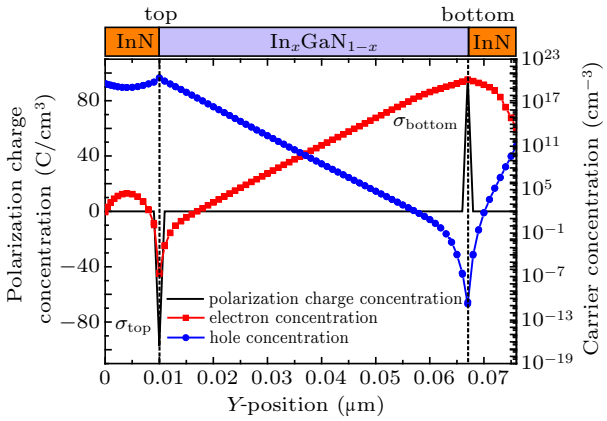


Fig. 3. Vertical distribution of carrier concentration and polarization charge concentration in source region and drain region along line D–D' in Fig. 1(b).

3. Results and discussion

3.1. Device performance of InN-Homo-TG-TFET and proposed InN-Hetero-TG-TFET

Figure 4 shows the transfer characteristic curves of the InN-Homo-TG-TFET ($\varphi = 5.65$ eV), InN-Homo-TG-TFET ($\varphi = 4.8$ eV), and proposed InN-Hetero-TG-TFET ($\varphi_0 = 5.65$ eV, $\varphi_1 = 4.8$ eV). As can be seen, both InN-Homo-TG-TFETs exhibit almost the same transfer characteristic curves, which is due to the fact that the change of work-function of the gate in the InN-Homo-TG-TFET can nearly only affect the threshold. Compared with the InN-Homo-TG-TFET, the InN-Hetero-TG-TFET shows a high I_{ON} of 4.45×10^{-5} A/μm at $V_{DS} = 0.5$ V and $V_{overdrive} = 0.5$ V. And, an I_{ON} of more than 10^{-4}A/μm can be achieved in the InN-Hetero-TG-TFET at $V_{DS} = 0.5$ V and $V_{overdrive} = 1$ V. Besides, the calculated SS_{avg} of the InN-Hetero-TG-TFET is 7.5 mV/dec which is much smaller than that of the InN-Homo-TG-TFET (39.4 mV/dec). As shown in the figure, all the three devices have almost the same good off-state characteristics, which lead to a higher I_{ON}/I_{OFF} of 10^{13} in the InN-Hetero-TG-TFET than that in the InN-Homo-TG-TFET (with I_{ON}/I_{OFF} of 10^{11}) at $V_{overdrive} =$ 0.5 V. These results demonstrate that the device with a hetero T-shaped gate possesses an excellent turn-on performance.

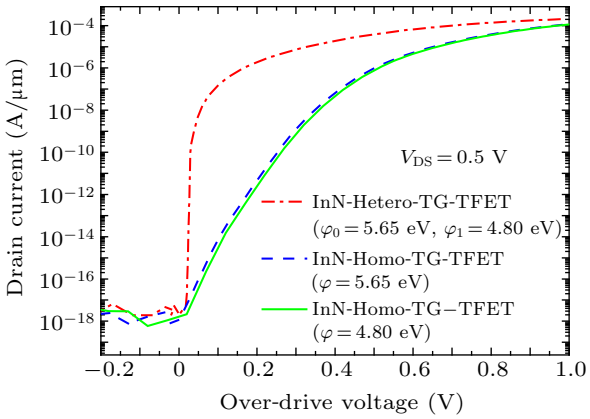


Fig. 4. Transfer characteristic curves of InN-Homo-TG-TFET ($\varphi = 5.65$ eV), InN-Homo-TG-TFET ($\varphi = 4.8$ eV), and proposed InN-Hetero-TG-TFET ($\varphi_0 = 5.65$ eV, $\varphi_1 = 4.8$ eV).

In order to reveal the tunneling mechanism of the proposed InN-Hetero-TG-TFET, figure 5 gives the contour of the nonlocal BTBT e-tunneling rate in the right half part of the InN-Homo-TG-TFET and proposed InN-Hetero-TG-TFET. As shown in Fig. 5, comparing with the InN-Homo-TG-TFET, a wide tunneling region along the line E–E' in Fig. 1(b) can be realized in the InN-Hetero-TG-TFET, which results in a wider one-dimensional tunneling rate profile in Fig. 6. And from Fig. 6 it is seen that the tunneling rate peak in the InN-Hetero-TG-TFET is much larger than that in the InN-Homo-TG-TFETs near the interface of InN/InGaN. Besides, the introduction of gate 1 can play an effective role in improving the tunneling rate near the bottom of gate trench in the InN-Hetero-TG-TFET. Because the integral of the area under each tunneling rate curve can represent the value of the tunneling current, the greater area under the tunneling rate curve in the InN-Hetero-TG-TFET indicates a greater tunneling current than in the InN-Homo-TG-TFET.

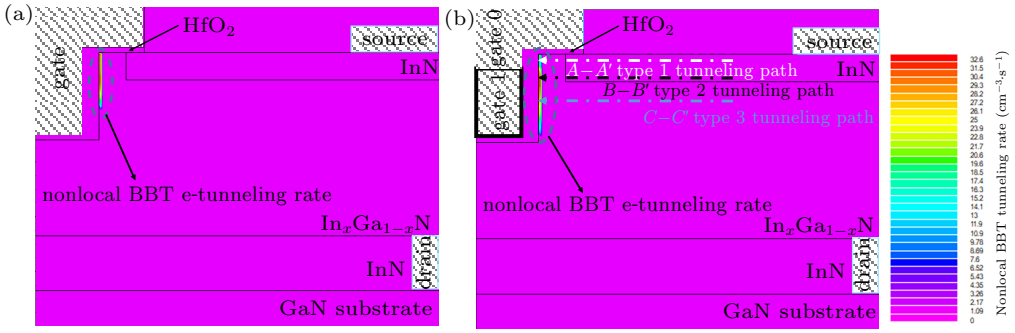


Fig. 5. Contours of nonlocal BTBT e-tunneling rate of half part of (a) InN-Homo-TG-TFET and (b) proposed InN-Hetero-TG-TFET when $V_{\text{overdrive}} = 0.5$ V and $V_{\text{DS}} = 0.5$ V.

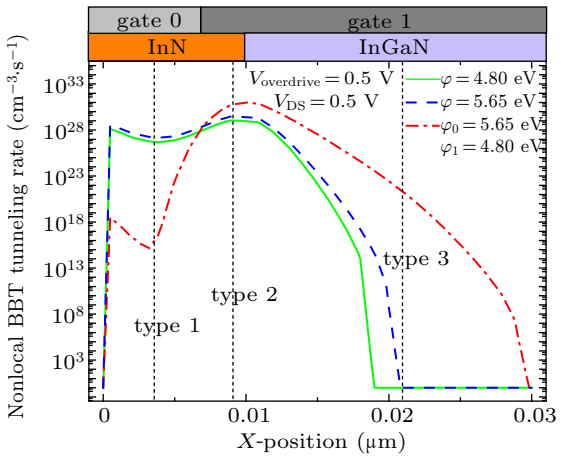


Fig. 6. One-dimensional distribution of nonlocal BTBT tunneling rate extracted from InN-Homo-TG-TFET ($\varphi = 5.65$ eV), InN-Homo-TG-TFET ($\varphi = 4.8$ eV), and proposed InN-Hetero-TG-TFET ($\varphi_0 = 5.56$ eV, $\varphi_1 = 4.8$ eV) when $V_{\text{overdrive}} = 0.5$ V and $V_{\text{DS}} = 0.5$ V along the line E–E' in Fig. 1(b).

In Fig. 5(b), there exist three typical types of tunneling paths in the InN-Hetero-TG-TFET. For the convenience of the analysis afterwards, the three typical types of tunneling paths are marked in Figs. 5(b) and 6, namely, along the line A–A' (type 1), line B–B' (type 2), and line C–C' (type 3) corresponding to Fig. 1(b). The type 1 and type 2 describe the tunneling from InN to InGaN under the control of gate 0 and gate 1, respectively. And the type 3 describes the tunneling path in InGaN under the control of gate 1.

Further explanation about the modulation mechanism of the hetero T-shaped gate is shown by Fig. 7. The arrowed lines represent the tunneling paths and tunneling distances in devices at on-state. Almost the same energy band of the InN-Homo-TG-TFETs with $\varphi = 5.56$ eV or $\varphi = 4.8$ eV can be seen, indicating the slight effect of the metal work-function on the performance. This is consistent with the result in Fig. 4.

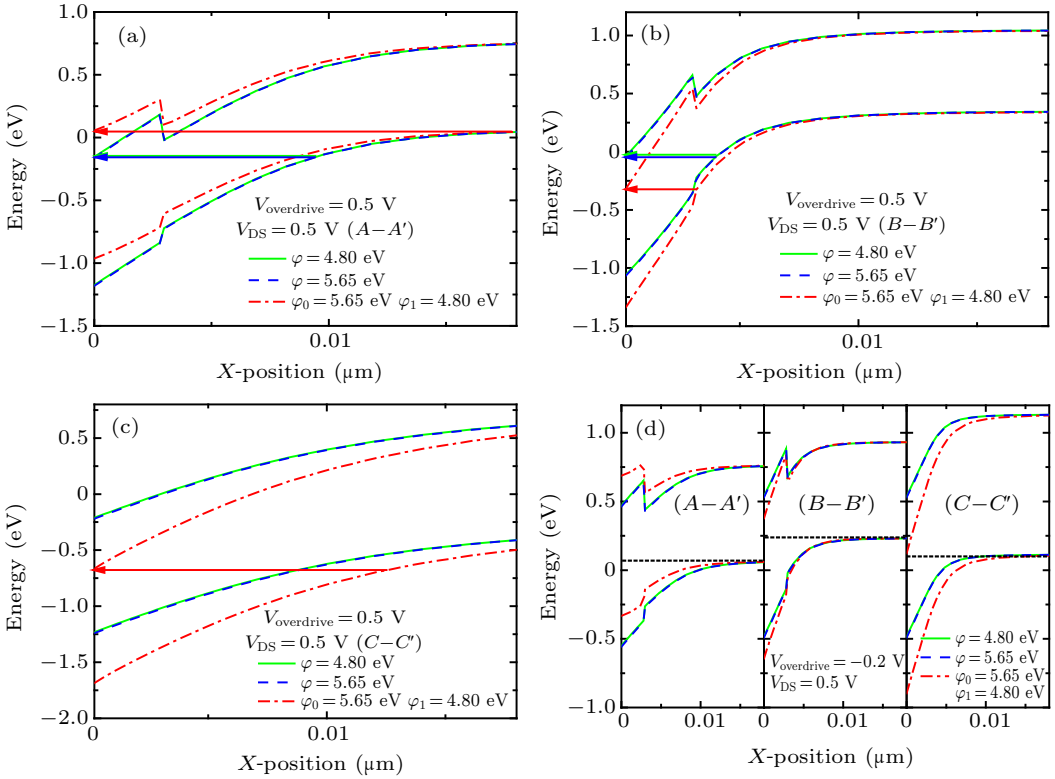


Fig. 7. Energy band of InN-Homo-TG-TFET ($\varphi = 5.56$ eV), InN-Homo-TG-TFET ($\varphi = 4.8$ eV), and proposed InN-Hetero-TG-TFET ($\varphi_0 = 5.56$ eV, $\varphi_1 = 4.8$ eV) along (a) line A–A', (b) line B–B', and (c) line C–C' in Fig. 1(b) when $V_{\text{overdrive}} = 0.5$ V, and $V_{\text{DS}} = 0.5$ V and (d) when $V_{\text{overdrive}} = -0.2$ V and $V_{\text{DS}} = 0.5$ V.

In Fig. 7, in all devices, the tunneling distances of type 2 are all less than 5 nm which are obviously smaller than those of types 1 and 3. It indicates a dominant effect of type 2 on the tunneling current. Because of the effective modulation effect of the hetero T-shaped gate, the tunneling distance of type 2 in the InN-Hetero-TG-TFET is shorter than that in the InN-Homo-TG-TFET, resulting in a greater tunneling rate and thus a larger tunneling current as well as a smaller average subthreshold swing in the InN-Hetero-TG-TFET. This accords well with the results in Figs. 4 and 6. Besides, nearly no tunneling can be seen for type 3 in InN-Homo-TG-TFETs, while there still exits a certain tunneling for type 3 in the InN-Hetero-TG-TFET, which further demonstrates an effective modulation effect of the bottom of gate trench in InN-Hetero-TG-TFET on the energy band. In Fig. 7(d), nearly no tunneling can be seen in all devices at off-state, which indicates a significantly small off-state leakage current. These results demonstrate excellent characteristics of the InN-Hetero-TG-TFET.

3.2. Influence of hetero T-shaped gate1 work-function φ_1 on InN-Hetero-TG-TFET

Figure 8 shows the influence of hetero gate1 work-function φ_1 on transfer characteristics in InN-Hetero-TG-TFET. As shown in the figure, the transfer curves shift towards the negative voltage direction when φ_1 decreases. And with the help of hetero gate, the SS_{avg} and I_{ON} can be improved efficiently. The variation extracted from Fig. 8(a) is shown in Fig. 8(b) and the corresponding energy band diagrams are also depicted in Fig. 9. It could be seen in Fig. 8(b) that I_{ON} continuously increases while SS_{avg} decreases with φ_1 decreasing. The results can be illustrated by the energy band diagrams in Fig. 9. As it is shown, the tunneling distance decreases with φ_1 decreasing and reaches a minimum value at $\varphi_1 = 4.70$ eV, which results in a highest I_{ON}. And, due to the improved modulation ability of the gate with φ_1 decreasing, the SS_{avg} keeps on falling. In order to achieve the enhancement mode device, $\varphi_1 = 4.8$ eV is chosen as the optimal value in the following.

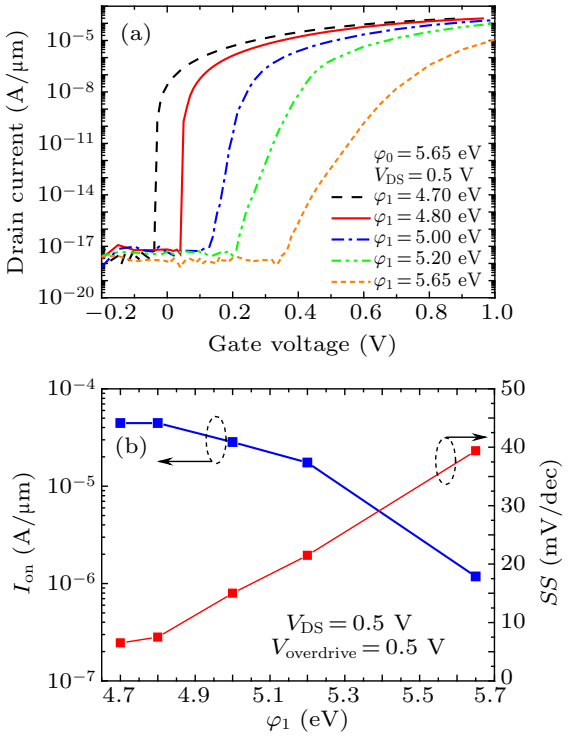


Fig. 8. Influence of hetero gate-1 work-function φ_1 on InN-Hetero-TG-TFET performance, showing (a) transfer characteristics and (b) extracted I_{ON} and SS_{avg}.

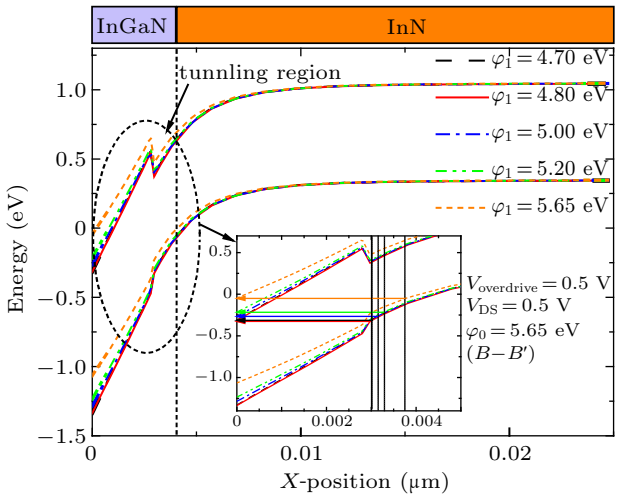


Fig. 9. Influence of hetero gate-1 work-function φ_1 on energy band of InN-Hetero-TG-TFET along line B–B' in Fig. 1(b) when $V_{DS} = 0.5$ V and $V_{overdrive} = 0.5$ V.

3.3. Influence of hetero T-shaped gate-0 work-function φ_0 on InN-Hetero-TG-TFET

Figure 10 shows the influence of hetero gate-0 work-function φ_0 on transfer characteristics in the InN-Hetero-TG-TFET. As it is shown, the transfer curves shift towards

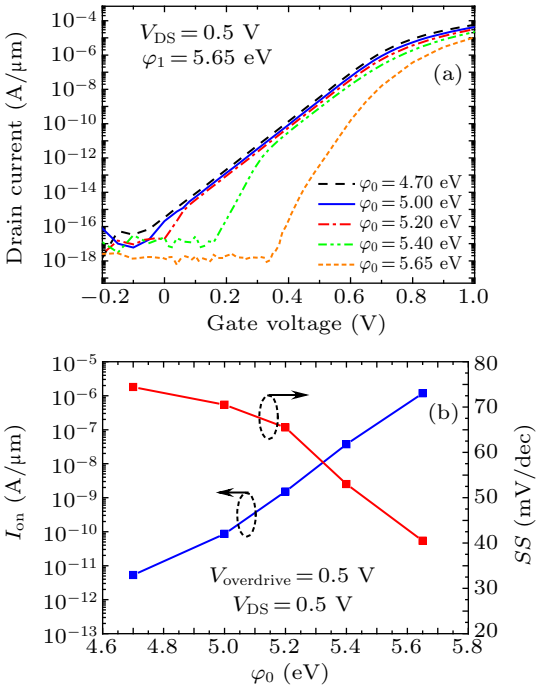


Fig. 10. Influence of hetero gate-0 work-function φ_0 on InN-Hetero-TG-TFET performance: (a) transfer characteristics and (b) extracted I_{ON} and SS_{avg}.

the negative voltage direction and the subthreshold characteristics are degraded gradually as φ_0 decreases. The variation extracted from Fig. 10(a) is shown in Fig. 10(b), and the corresponding energy band diagrams are also depicted in Fig. 11. It could be seen in Fig. 10(b) that I_{ON} decreases and SS_{avg} increases with φ_0 decreasing, which is attributed to the increase in tunneling distance as shown in Fig. 11. Therefore, $\varphi_0 = 5.56$ eV is adopted in the following investigation.

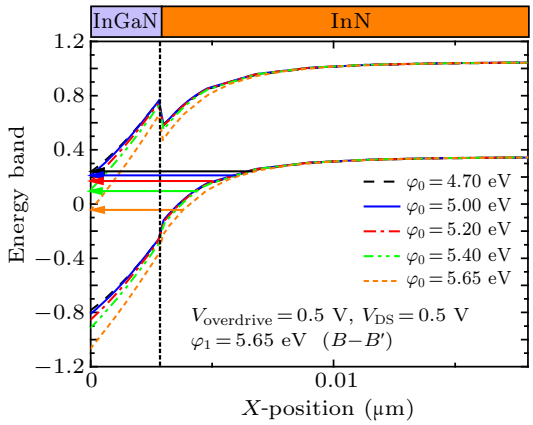


Fig. 11. Influence of hetero gate-0 work-function φ_0 on energy band of InN-Hetero-TG-TFET along line B–B' in Fig. 1(b) when $V_{DS} = 0.5$ V and $V_{overdrive} = 0.5$ V.

3.4. Influence of hetero T-shaped gate position T_{g1} on InN-Hetero-TG-TFET

The influence of hetero gate-1 thickness T_{g1} on the performance of InN-Hetero-TG-TFET is shown in Fig. 12 and the corresponding energy band diagrams are shown in Fig. 13. As shown in Fig. 12, the transfer curves shift towards the negative voltage direction when T_{g1} is raised. And I_{ON} increases continuously with T_{g1} increasing. Based on the energy band in Fig. 13, the energy band on gate side will shift down with T_{g1} increasing, which can shorten the tunneling distance and increase the tunneling rate, resulting in the variation of I_{ON}. It can be observed that SS_{avg} first decreases and then increases but reaches a minimum value at $T_{g1} = 23$ nm. This is due to the changing of modulation ability of the hetero gate around $T_{g1} = 23$ nm. With T_{g1} increasing, the modulation ability of the whole hetero gate (gate 0 and gate 1) converts from that of the high metal work-function homo gate to that of hetero gate, then to that of the low metal work-function homo gate, which results in the trend of SS_{avg}. Based on these analyses, it is important to find the balance point of T_{g1}, and T_{g1} is chosen to be 23 nm for the proposed device in this paper. The characteristics of the proposed device in comparison with those of our previous reported lateral PI-InN-TFET and the state-of-the-art III-nitride-based TFETs are given in Table 3, which demonstrates the excellent performance of InN-Hetero-TG-TFET.

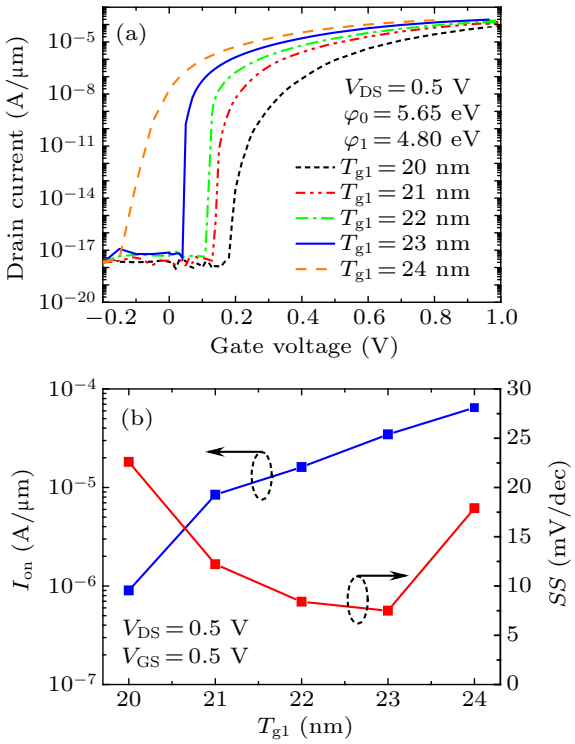


Fig. 12. Influence of hetero gate-1 thickness T_{g1} on InN-Hetero-TG-TFET performance for total gate trench thickness T_{gate} of 30 nm, showing (a) transfer characteristics and (b) extracted I_{ON} and SS_{avg}.

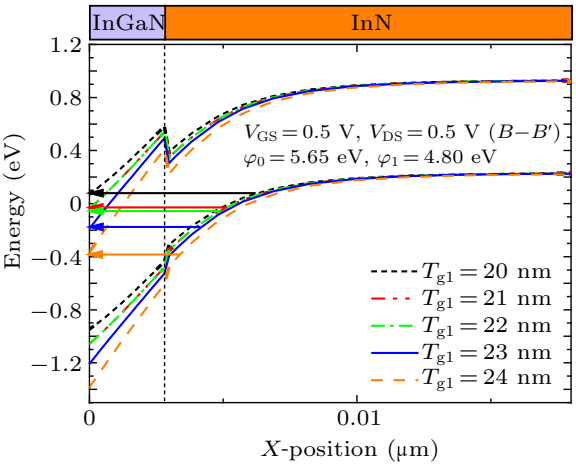


Fig. 13. Influence of hetero gate-1 thickness T_{g1} on energy band along line B–B' in Fig. 1(b) when $V_{DS} = 0.5$ V and $V_{GS} = 0.5$ V.

Table 3. Comparison of characteristic between proposed device and state-of the-art nitride TFETs.

Devices	I_{ON} (A/μm)	SS_{avg} (mV/dec)	I_{ON}/I_{OFF} ratio
InGaN GEDL-TFETs[16] @$V_{DS} = 0.5$ V	8.02×10^{-5}	7.9	10^{13}
NW TFETs[18] @$V_{DS} = 0.5$ V	5×10^{-5}	25	10^{11}
Our previous PI-InN-TFET[31] @$V_{DS} = 0.5$ V	1.5×10^{-5}	33	10^{12}
InAlN/InGaN TFETs[35] @$V_{DS} = 0.5$ V	7.85×10^{-4}	< 60	10^{7}
Proposed TFEF @$V_{DS} = 0.5$ V	1×10^{-4}	7.5	10^{13}

4. Conclusions

In this paper, we present a new vertical polarization-induced doping InN/InGaN heterojunction tunnel FET with hetero T-shaped gate (InN-Hetero-TG-TFET). The proposed device can realize the drain and source region doping by means of polarization effect without the conventional physical doping processing, which can avoid the random dopant fluctuation (RDF) and the problems related to the high thermal annealing techniques in the conventional physical doping tunnel FETs. In addition, the improvement of the I_{ON} and SS_{avg} can be achieved, benefitting from the utilization of the hetero T-shaped gate with different metal work-functions. The device electrical characteristics and the physical mechanisms are studied systematically. Simulation results demonstrate the excellent performance of InN-Hetero-TG-TFET in comparison with those of the InN-Homo-TG-TFET and our previously reported lateral polarization-induced InN-based TFET (PI-InN-TFET), which could provide an effective method for the further development of TFETs.

References

[1] Ionescu A M and Riel H 2011 *Nature* **479** 329
[2] Seabaugh A and Zhang Q 2010 *Proc. IEEE* **98** 2095
[3] Zhang S L, Liang R R, Wang J, Tan Z and Xu J 2017 *Chin. Phys. B* **26** 018504
[4] Li C, Yan Z R, Zhuang Y R, Zhao X L and Guo J M 2018 *Chin. Phys. B* **27** 078502
[5] Ionescu A M, De Michielis L, Dagtekin N, Salvatore G, Cao J, Rusu A and Bartsch S 2011 *IEEE International Electron Devices Meeting (Iedm)*, December 5–7, 2011, Washington, DC, USA, p. 16.1.1
[6] Choi W Y, Park B G, Lee J D and Liu T J K 2007 *IEEE Electron Dev. Lett.* **28** 743
[7] Ghosh B and Akram M W 2013 *IEEE Electron Dev. Lett.* **34** 584
[8] Vijayvargiya V and Vishvakarma S K 2014 *IEEE Trans. Nanotechnol.* **13** 974
[9] Chiang M H, Lin J N, Kim K and Chuang C T 2007 *IEEE Trans. Electron Dev.* **54** 2055
[10] Damrongplasit N, Shin C, Kim S H, Vega R A and Liu T J K 2011 *IEEE Trans. Electron Dev.* **58** 3541
[11] Damrongplasit N, Kim S H and Liu T J K 2013 *IEEE Electron Dev. Lett.* **34** 184
[12] Leung G and Chui C O 2013 *IEEE Trans. Electron Dev.* **60** 84
[13] Kumar M J and Janardhanan S 2013 *IEEE Trans. Electron Dev.* **60** 3285
[14] Hueting R J E, Rajasekharan B, Salm C and Schmitz J 2008 *IEEE Electron Dev. Lett.* **29** 1367
[15] Tirkey S, Sharma D, Raad B R and Yadav D S 2018 *IEEE Trans. Electron Dev.* **65** 282
[16] Duan X L, Zhang J C, Wang S L, Li Y, Xu S R and Hao Y 2018 *IEEE Trans. Electron Dev.* **65** 1223
[17] Li W J, Sharmin S, Ilatikhameneh H, Rahman R, Lu Y Q, Wang J S, Yan X D, Seabaugh A, Klimeck G, Jena D and Fay P 2015 *IEEE J. Explor. Solid-State Computat. Devices Circuits* **1** 28
[18] Li W J, Cao L N, Lund C, Keller S and Fay P 2016 *Phys. Status Solidi A* **213** 905
[19] Simon J, Zhang Z, Goodman K, Xing H L, Kosel T, Fay P and Jena D 2009 *Phys. Rev. Lett.* **103** 026801
[20] Krishnamoorthy S, Nath D N, Akyol F, Park P S, Esposto M and Rajan S 2010 *Appl. Phys. Lett.* **97** 203502
[21] Chaney A, Turski H, Nomoto K, Wang Q X, Hu Z Y, Kim M, Xing H G and Jena D 2018 *76th Device Research Conference (DRC)*, June 24–27, 2018, Santa Barbara, USA, pp. 1–3
[22] Mao W, Peng Z L, Yang C, Wang H Y, Du M, Wang X F, Zheng X F, Wang C, Zhang J C and Hao Y 2019 *Semicond. Sci. Technol.* **34** 065015
[23] Ilatikhameneh H, Ameen T A, Klimeck G, Appenzeller J and Rahman R 2015 *IEEE Electron Dev. Lett.* **36** 1097
[24] Yang Z N 2016 *IEEE Electron Dev. Lett.* **37** 839
[25] Lin J T, Wang T C, Lee W H, Yeh C T, Glass S and Zhao Q T 2018 *IEEE Trans. Electron Dev.* **65** 769
[26] Krishnamohan T, Kim D, Raghunathan S and Saraswat K 2008 *IEEE International Electron Devices Meeting (IEDM)*, December 15–17, 2008, San Francisco, CA, USA, pp. 1–3
[27] Saurabh S and Kumar M J 2011 *IEEE Trans. Electron Dev.* **58** 404
[28] Seabaugh A, Fathipour S, Li W J, Lu H, Park J H, Kummel A C, Jena D, Fullerton-Shirey S K and Fay P 2015 *IEEE International Electron Devices Meeting (IEDM)*, December 7–9, 2015, Washington, DC, USA, p. 35.6.1
[29] Chang H Y, Adams B, Chien P Y, Li J P and Woo J C S 2013 *IEEE Trans. Electron Dev.* **60** 92
[30] Wang P F, Hilsenbeck K, Nirschl T, Oswald M, Stepper C, Weis M, Schmitt-Landsiedel D and Hansch W 2004 *Solid State Electron.* **48** 2281
[31] Mao W, He Y H, Yang C, Wang H Y, Du M, Zheng X F, Wang X F, Wang C, Zhang J C and Hao Y 2020 *Semicond. Sci. Technol.* **35** 075012
[32] Ghosh K and Singisetti U 2014 *IEEE Trans. Electron Dev.* **61** 3405
[33] Vurgaftman I, Meyer J R and Ram-Mohan L R 2001 *J. Appl. Phys.* **89** 5815
[34] Wang T, Wang X Q, Chen Z Y, Sun X X, Wang P, Zheng X T, Rong X, Yang L Y, Guo W W, Wang D, Cheng J P, Lin X, Li P, Li J, He X, Zhang Q, Li M, Zhang J, Yang X L, Xu F J, Ge W K, Zhang X X and Shen B 2018 *Adv. Sci.* **5** 1800844
[35] Ameen T A, Ilatikhameneh H, Fay P, Seabaugh A, Rahman R and Klimeck G 2019 *IEEE Trans. Electron Dev.* **66** 736